The International Journal of Advanced Manufacturing Technology (2023) 128:891–901
https://doi.org/10.1007/s00170-023-11950-9

ORIGINAL ARTICLE

Inconel 718 produced by hot pressing: optimization of temperature and pressure conditions

Ana Marques[1,2] · Ângela Cunha[1,2] · Flávio Bartolomeu[1,2] · Filipe Samuel Silva[1,2] · Óscar Carvalho[1,2]

Received: 20 January 2023 / Accepted: 12 July 2023 / Published online: 21 July 2023

Abstract

This paper aims to act as a useful engineering tool for researchers who are studying the production of well-densified IN718 parts by uniaxial vacuum hot pressing. To the best of the authors' knowledge, there is no relevant information on literature about densification of IN718 parts by this technique. This work is focused on understanding the influence of uniaxial vacuum hot pressing sintering conditions (temperature and pressure) on Inconel 718 (IN718) powder densification, microstructural, fracture mode, and hardness properties. The optimization of temperature and pressure sintering conditions are presented as well as its influence on the densification, microstructural features, and hardness properties. The sintering conditions included temperatures of 1000, 1068, 1150, and 1200 °C; pressures of 50 and 60 MPa; and a dwell time of 60 min.

The results showed an increase in the grain size (GS) of the compacts with the processing temperature and a change on the fracture mode from intergranular dominant fracture to fully dimple ductile fracture. Regarding the microstructural properties, the results showed that $\gamma'(Ni_3(Al, Ti))$ intermetallic precipitate originated from IN718 powders was retained in the sintered specimens. The hardness results revealed that the sintering temperature of 1000 °C is not enough to promote accurate densification. The optimum hardness results were achieved at 1200 °C (327 HV) with high levels of densification and pure intragranular fracture mode. In future studies, shear and tensile strength test should be performed in order to properly evaluate the mechanical behavior of hot-pressed IN718 specimens.

Keywords Inconel 718 · Powder · Metallurgy · Hot pressing · Densification · Microstructure · Fracture · Hardness

1 Introduction

The aerospace components are usually under severe operating conditions and require high-strength alloys (such as Inconel alloys) with resistance to high temperature, pressure, and corrosion conditions [1–4]. Inconel 718 (IN718) is one of the most used alloys in this field and has been reported as suitable for being processed by powder metallurgy (PM) techniques. This alloy allows to add up significant amounts of precipitated strengthening elements without considerable segregation, during the atomization procedures. The PM field includes some techniques in which metal or ceramic powders are, simultaneously, compressed and heated till reaching a suitable temperature for powder densification but lower than the materials' melting points. Usually, the process starts with powder atomization, followed by cold compaction, and finally, the densification of the powders occurs within a mold (under high pressure and temperature conditions) [2, 5–7].

The main powder metallurgy techniques reported in literature are hot pressing (HP), hot isostatic pressing (HIP), metal extrusion, metal injection molding, and rolling technologies [6, 8, 9]. Hot isostatic pressing is a propitious technology since it allows to obtain consolidated parts with high densification levels and high mechanical properties (when compared with other conventional processes) [7, 10, 11]. The HIPed parts are produced directly from the powders and are usually obtained with a homogeneous microstructure which is beneficial for improving the mechanical properties [7–9, 12, 13]. Chang et al. [8] produced IN718 parts by hot isostatic pressing considering four sintering pressures (98.6, 147.9, 172.6, and 197.2 MPa) under 1180 °C of sintering

✉ Ana Marques
anacristinamarques95@gmail.com

[1] CMEMS – Center for Microelectromechanical Systems, University of Minho, Azurém, 4800-058 Guimarães, Portugal

[2] LABBELS – Associate Laboratory, Guimarães, Braga, Portugal

temperature for 2 h. Regarding the physical and microstructural properties, the optimum sintering pressure was found to be 172.6 MPa since the porosity results decreased 78.5% and reduced the amount of δ precipitation. In coherence with these results, the tensile strength results were improved in 18.5% at room temperature. Chang et al. [14] also investigated the precipitation of carbides and oxides on the prior particle boundaries which led to a decrease in the mechanical properties. The tensile fracture mode changed when the temperature was increased because the prior particle boundaries have been dissociated with the carbide particles. The fracture mode was classified as interparticle dominant fracture, at room temperature, and was modified to entirely dimple fracture with the increase of temperature.

Hot-pressing technology has been reported as a successful sintering method that allows to obtain highly densified parts with mechanical properties close to the theoretical values. This sintering technique is usually applied as a post-treatment in consolidated parts as well as to promote diffusion and bonding of distinct materials. The high sintering temperature is extremely important for enhancing the plastic deformation and therefore promotes an efficient particle bonding. The applied pressure and the surface energy of the particles stimulate a driving force that leads to a rapid densification [15]. The high-temperature resistance of IN718 makes it a difficult alloy to be sintered when compared with other materials. The main purpose of this work is to act as a useful engineering tool for researchers who are investigating the sintering conditions and mechanisms of as-produced IN718 parts by uniaxial vacuum hot pressing since, to the best of the authors' knowledge, there is no relevant information on literature about this topic. The optimization of temperature and pressure sintering conditions are presented as well as its influence on the densification, microstructural features, and hardness properties.

2 Materials and methods

2.1 Powder's features

IN718 powder morphology (Fig. 1a) was analyzed by an analytical scanning electron microscope (JEOL JSM-6010LV). The powders used in this study were purchased from Carpenter Additive supplier with a given particle size ranging between 15 and 45 µm (confirmed by the grain size distribution presented in Fig. 1b). However, most of the particle sizes are between 20 and 35 µm, and some of them revealed some satellites on the surface (Fig. 1a).

IN718 is a Ni–Fe–Cr alloy with 50.0–55.0% Ni and 21.0% Cr that avoid oxidation at high temperatures (Table 1). The molybdenum (Mo) is also a constituent of this alloy (2.8–3.3%) that is responsible for avoiding pitting corrosion [16]. Other elements such as titanium, aluminum, cobalt, and iron are also presented in this alloy. Moreover, the solubility of chromium, tungsten, iron, molybdenum, and cobalt on the austenitic matrix (γ) enhances the mechanical strength [17].

The XRD graphic of IN718 powder (Fig. 2) revealed the main presence of γ (111) plane and a solid solution of austenite (γ) with a face-centered cubic (fcc) Ni–Cr matrix.

2.2 Uniaxial vacuum hot pressing

IN718 specimens were manufactured through hot-pressing technique that includes a vacuum sintering system (at a pressure of 10^{-2} mbar) and induction furnace with high frequency. The experimental procedure started with the weight of the IN718 powders, and the covering of the graphite die surface with ZrO_2 paste to avoid an invisible diffusion of the carbon on the hot-pressed specimen. The IN718 powders were introduced into the graphite die and were positioned into the hot-pressing chamber for further assembly in hot pressing

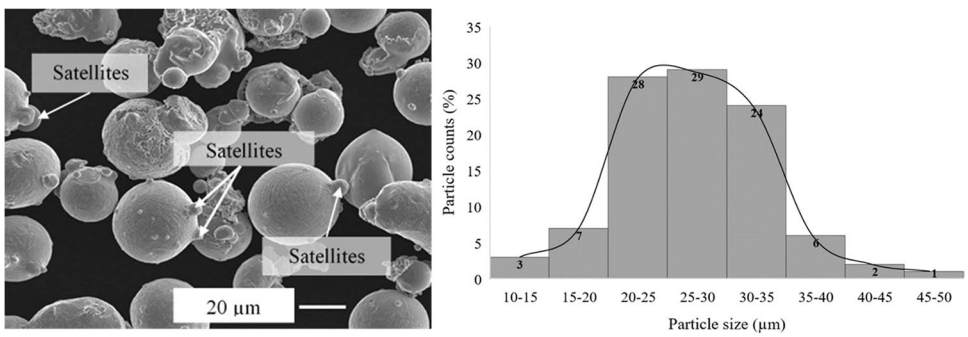

Fig. 1 IN718 alloy powders: **a** SEM image and **b** particle size distribution

Table 1 Chemical composition of IN718 powder (Carpenter Additive Lda) [18]

Elements	Al	Cr	Co	Cu	Fe	Mn	Mo	Ni	Nb + Ta	Si	Ti
wt.%	0.70	21	1	0.3	Balance	0.35	2.80–3.30	50–55	4.75–5.50	0.15	1.15

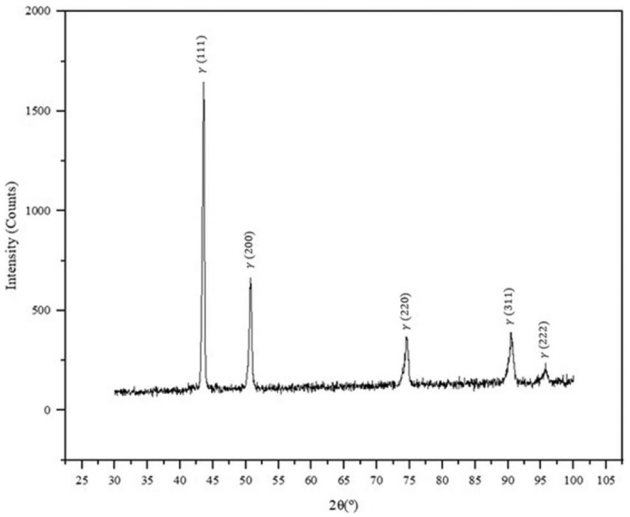

Fig. 2 XRD pattern of IN718 powder: the presence of a solid solution of austenite (γ)

structure. A thermocouple was inserted into the graphite die (close to the specimen) to monitor the temperature (Fig. 3).

The procedure started by applying a heating rate of about 5 °C/s till the final temperature. When the temperature reaches 80% of the final temperature, the defined uniaxial pressure is applied and kept during the stage time (60 min), as represented in Fig. 4. After the specimens cool down (till room temperature), the final parts were removed from the graphite die. The IN718 powders were simultaneously heated and pressed, boosting the atomic diffusion of the particles and increasing the densification of the specimens.

Usually, hot pressing is characterized by using 75–80% of the melting temperature of the materials, and in this sense, this temperature was first defined. As the appropriate hot-pressing sintering temperature conditions are not yet reported in literature, the first temperature considered was 75% of the melting point of IN718 (1260–1336 °C) [19]. Chang et al. [8] studied the densification of IN718 specimens by HIP, at a temperature of 1180 °C, and considered higher pressure values (98.6–197.2 MPa) than those allowed by the hot-pressing equipment used in this work (maximum of 60 MPa). In order to compensate the lower pressure values, higher sintering temperatures were added to the previously mentioned temperature (1068°C, 1150 °C, and 1200 °C which correspond to approximately 80, 85, and 89% of the melting point) as can be seen in Table 2. Regarding the pressure conditions, two values were tested: 50 and 60 MPa, in order to evaluate the influence of pressure on densification level.

2.3 Characterization techniques

After the specimen's production by hot pressing, the IN718 specimens were extracted from the graphite die and polished using silicon carbide abrasive papers till 4000 mesh grit sand with a uniform thickness reduction. Specimens were ultrasonic cleaned with pure ethanol and acetone and afterward dried in

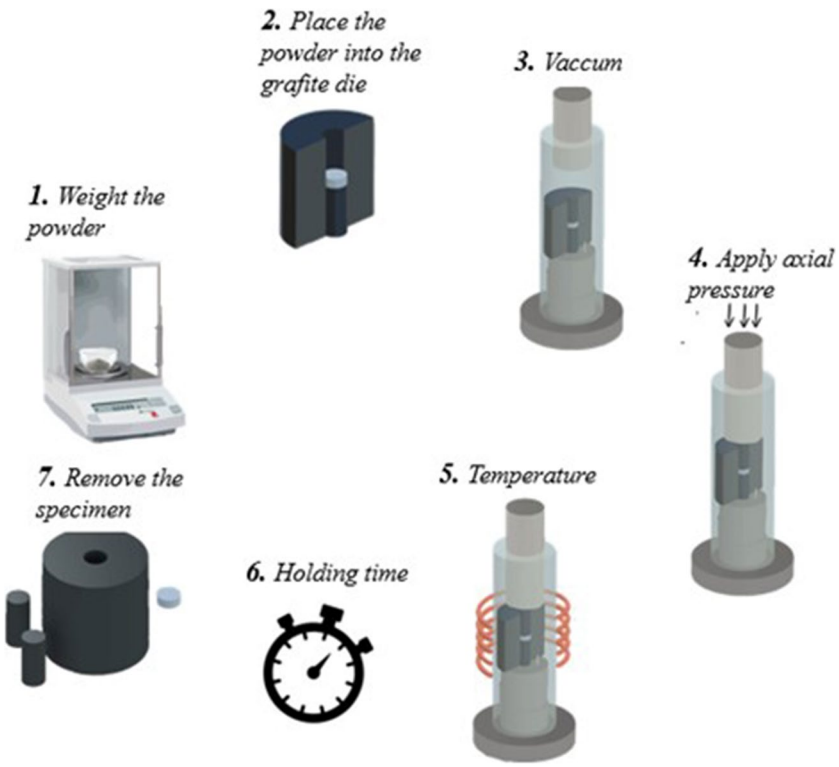

Fig. 3 Uniaxial vacuum hot pressing: a scheme of the main steps for producing IN718 specimens

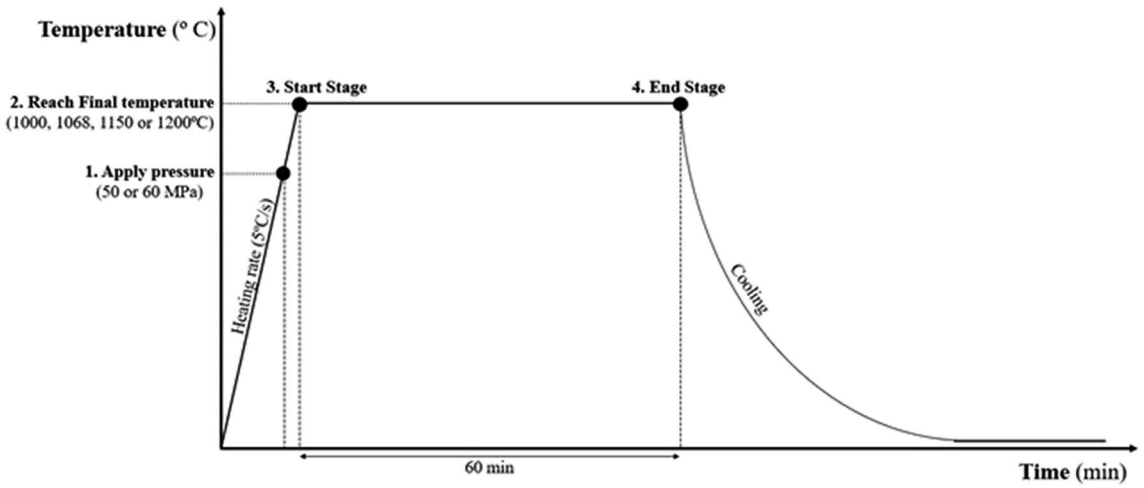

Fig. 4 Schematic representation of hot-pressing cycle employed to produce IN718 specimens

Table 2 Description of the hot-pressing sintering conditions

Designation	Temperature (°C)	Pressure (MPa)
T1000P50	1000	50
T1000P60		60
T1068P50	1068	50
T1068P60		60
T1150P50	1150	50
T1150P60		60
T1200P50	1200	50
T1200P60		60

air. An analytical scanning electron microscope (JEOL JSM-6010LV) was used for analyzing the powder and the grain morphology. The chemical etching solution Kallings No. 2 was used for assessing the grain morphology. This solution is composed by 10 HCl (37%), 10 ml ethanol, 10 ml H_2O, and 0.5 g $CuCl_2$ for 3 min. The IN718 specimens were fractured (without effect of a polishing or cutting tool) to evaluate the densification level.

X-ray diffraction (XRD) analysis was performed through a Bruker D8 Discover diffractometer with classical θ–2θ analysis with a Bragg–Brentano geometry utilizing CuKα radiation. This analysis considered 2θ (ranging between 30° and 100°), a 4 s/step of step time, and 0.04° of step size.

The weight and volume of each IN718 specimen were measured, and the conventional formula ($\rho = m / V$ [g/cm^3]) was used for estimating the density of the as-produced specimens. An EMCO-TEST (DuraScan model) equipment was used for measuring the microhardness of the specimens (1000 g for 15 s). The hardness measurements were performed from the periphery to the center of the specimen in order to evaluate its homogeneity.

3 Results and discussion

This chapter explains the densification and fracture mode of the specimens, then the grain morphology and microstructural features and finally the hardness properties.

3.1 Densification

The high level of densification of specimens is dependent on atomic diffusion and plastic deformation mechanisms. The simultaneous occurrence of these two phenomena leads to deformation of the polycrystalline aggregates, enhancing the grain growth and recrystallization. The density and densification results (Table 3) allowed us to verify that the density results of the hot-pressed IN718 specimens were closer to the theoretical values (8.20 g/cm^3 [20]) with densification results close to 100%.

The densification works through particle rearrangement and plastic flow at the particle contacts. At 1000 °C, the temperature is not enough to potentiate the plastic deformation. The driving force for densification was not enough for reducing the surface area energy associated with pores.

The IN718 specimens revealed a significant increase in densification level with the increase of temperature (from 94.59 to 99.88%, at 50 MPa). ElRakayby et al. [21] studied the densification of nickel base alloy powder under hot isostatic pressing and also verified an increase on densification with temperature. For temperature of 1150 and 1200 °C, the increase on temperature led to a significant increase on densification level for about 99%. At this temperature, bonding mechanisms such as diffusion, plastic flow, recrystallization, and others were strongly potentiated.

For all temperature conditions, the increase of pressure from 50 to 60 MPa led to an increase on densification of approximately 1%. High pressure induces compressive stress on powders that drives diffusion and/or dislocation motion.

Table 3 Estimated density and densification of the IN718 specimens manufactured by hot pressing

Designation	Estimated density (g/cm^3)	Densification (%)
T1000P50	7.75	94.591
T1000P60	7.99	97.544
T1068P50	7.82	95.440
T1068P60	7.91	96.553
T1150P50	8.03	98.001
T1150P60	8.18	99.772
T1200P50	8.189	99.877
T1200P60	8.197	99.969
Theoretical values	8.20 [20]	100

3.2 Fracture mode

The fracture surface images (represented in Fig. 5) allowed us to infer about the densification of the IN718 specimens by hot pressing. The ductile fracture mode was identified in all sintering conditions with substantial plastic deformation. Typically, IN718 fracture surface exhibits a ductile fracture mode which can be classified as intergranular or intragranular. However, some IN718 specimens also showed combination of two ductile fracture modes.

The fracture surface of the T1000P50 specimen revealed a pure intergranular fracture mode. The entire split up of the IN718 particles occurred because the grains were weakly bonded, and so, the cracks tend to propagate alongside the grain boundaries. The fracture surface images showed that

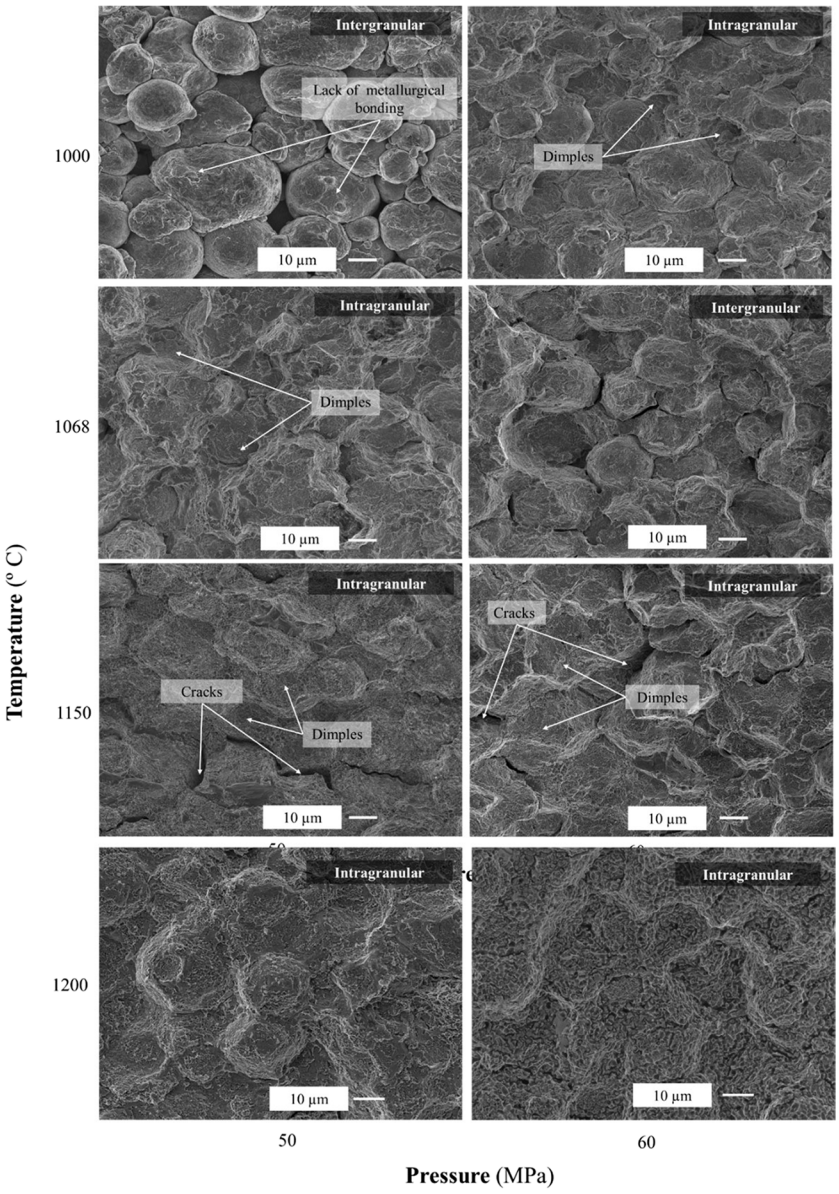

Fig. 5 Fracture surfaces of hot-pressed IN718 specimens at 1000 °C, 1068 °C, 1150, °C, and 1200 °C and 50 and 60 MPa

the increase in the pressure values (from 50 to 60 MPa) has influenced the powder's consolidation since the powders' contact area was enhanced. Hereupon, the T1000P60 specimen showed an intragranular fracture mode with some signs of intergranular mode (Fig. 5).

The increase in temperature (from 1000 to 1068 °C) showed a substantial impact on the particles' consolidation, leading to a good metallurgical bonding when compared with hot-pressed specimens at 1000 °C. The specimens produced at 1068 °C (considering both 50 and 60 MPa) presented an intragranular fracture mode in which the decohesion of particle boundary occurs alongside the dimples (resultant from high plastic deformation and atomic diffusion). The increase of pressure (from 50 to 60 MPa) led to obtain fracture surfaces with more clear plastic deformation. The fracture surfaces of T1068P60 specimen showed some voids that may have been created by external loads or grain boundary precipitates that were oxidized [22]. A ductile intragranular fracture mode was observed when considering the highest sintering temperature in this study (1150 °C), for both 50 and 60 MPa pressure conditions. However, it was possible to observe some cracks which means that the sintering conditions may not be enough to achieve the optimized level of consolidation. When increasing the sintering temperature to 1200 °C, a ductile intragranular fracture surface of specimens revealed a significant improvement in metallurgical bonding. A dimple fracture is observed since high levels of atomic diffusion and plastic deformation were achieved [23].

3.3 Microstructural analysis

Figure 6 shows the XRD patterns of IN718 powder and hot-pressed IN718 specimens. The XRD pattern is coincidental to the solid solution of austenite (γ) constituted by a single-phased structure with Ni, Cr, and Fe as the three most important elements. γ' and γ'' phases are the principal strain strengthening mechanisms [24]. The hot-pressed IN718 specimens did not show the presence of the γ'' strengthening phase since they have been processed at a lower temperature than its solvus temperature (900–920 °C) [25]. Nevertheless, the XRD patterns showed a steady strengthening γ' (Ni_3(Al, Ti) from IN718 powder. It is important to highlight that this phase is extremely relevant for improving the strength of IN718 parts that usually require high mechanical strength and corrosion resistance in large temperature range. The rapid precipitation of γ' (Ni_3(Al, Ti) phase enhances the mechanical strength although its low growth rate turns into a secondary strengthening phase when compared with γ'' (Ni_3Nb). Chromium carbides ($Cr_{23}C_6$) are formed by Cr precipitation which is driven by the increase on the sintering temperature. These carbides were coincidental with γ at 44° of the XRD pattern, when

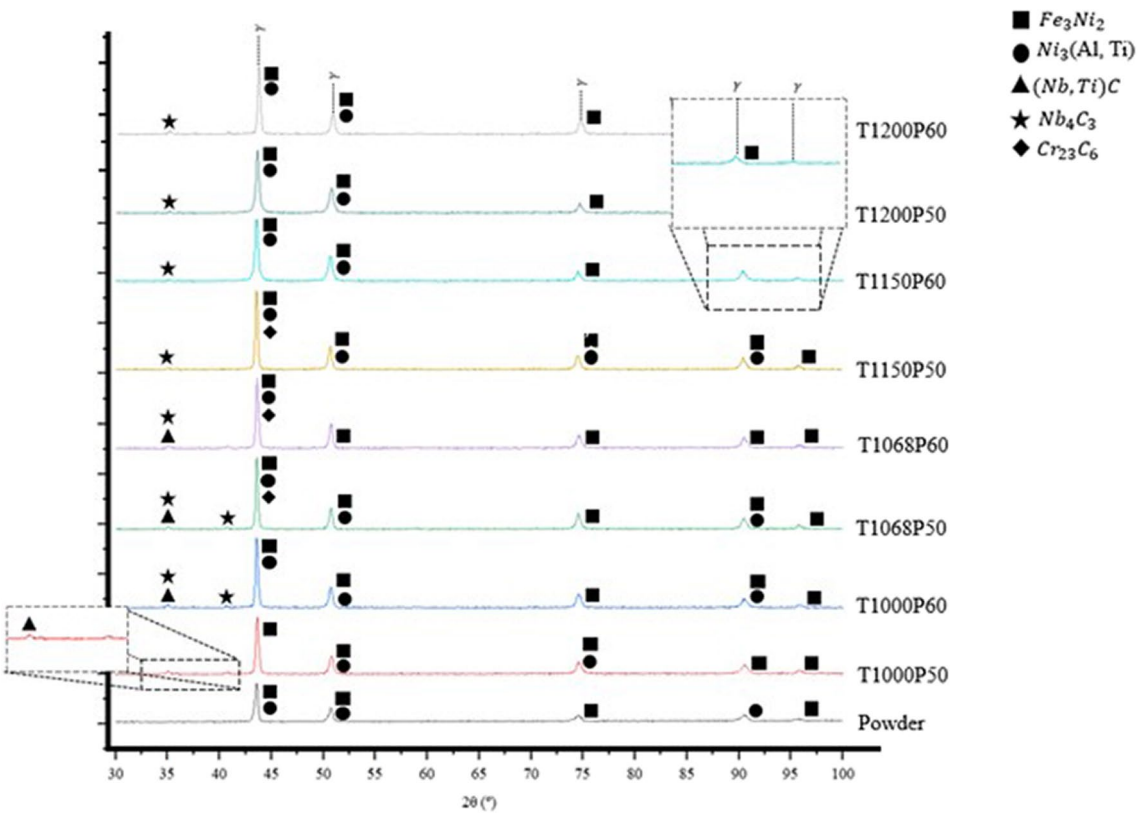

Fig. 6 XRD patterns of hot-pressed IN718 specimens

considering 1068 and 1150 °C temperatures even though the amount of Cr carbides has tended to reduce with the increase of temperature due to its dissolution into the γ matrix [26].

The formation of precipitates is highly dependent of the niobium (Nb) segregation which is strongly predisposed to this phenomenon. The low solidification rate, during hot pressing, is probably to enrich the macrosegregation of the Nb and formation of unwanted phases such as (Nb, Ti) C. However, these Nb carbides have been reported as advantageous for enhancing hardness properties [27]. XRD patterns showed distinct Nb carbides—Nb_4C_3 and (Nb, Ti) C—at 35 and 40° when IN718 powder was sintered from 1000 to 1200 °C. XRD patterns of IN718 powder did not show Nb carbides since these phases were created during solidification. As the melting point of this phase (3600 °C) is considerably higher than the IN718 melting point (1260–1336 °C [19]), this phase is described as a stable phase.

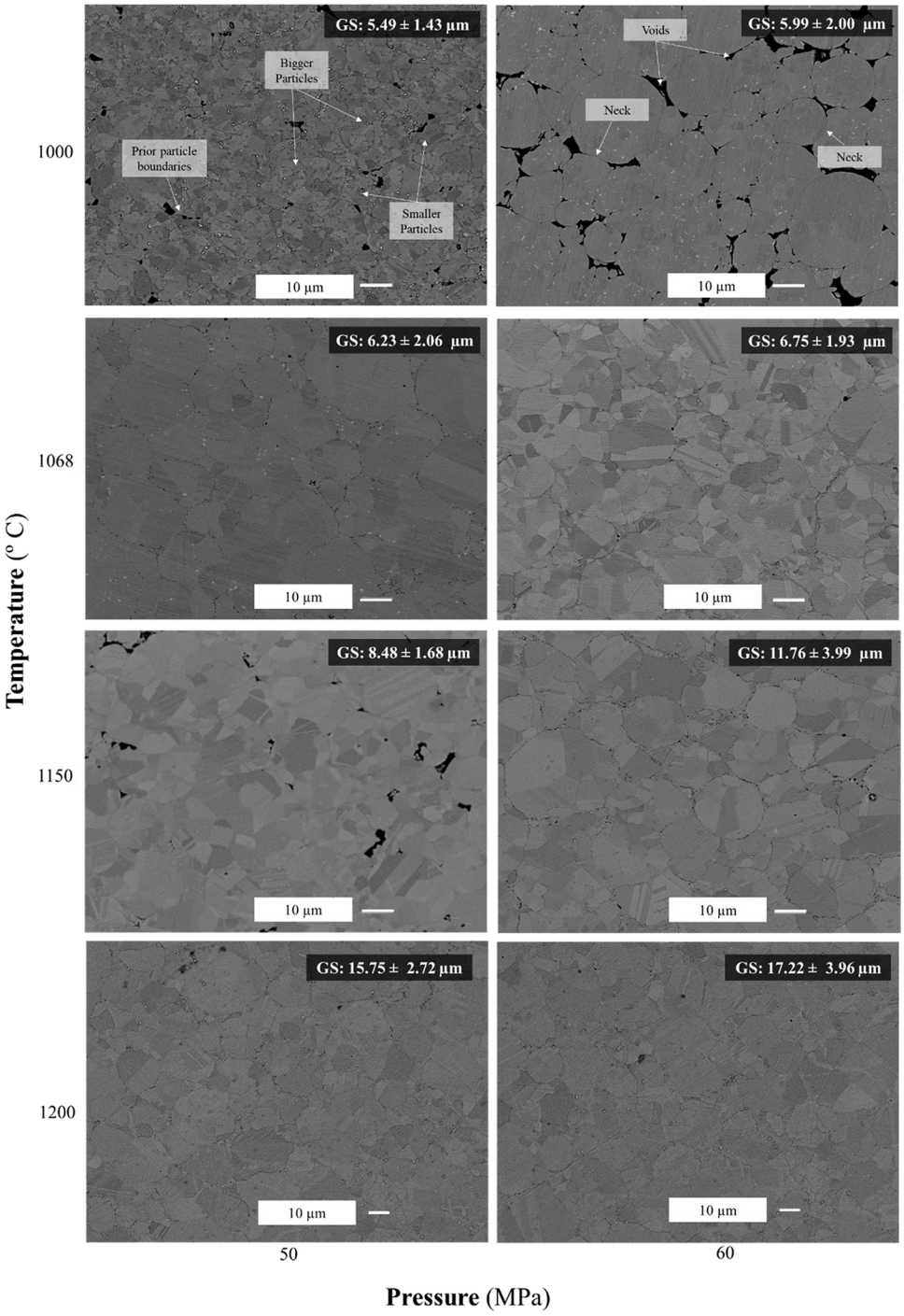

Fig. 7 Grain morphology of hot-pressed IN718 specimens considering different sintering conditions

3.4 Grain morphology

Both densification and hardness features can be inferred by the specimen's grain morphology, and for this reason, the effect of pressure and temperature processing parameters on the grain characteristics were studied (Fig. 7). During the solidification, the grain can be in two distinct stages. The first one is nucleation, in which stable nuclei are created and the second is the growth of nuclei which generates crystals and develops a grain structure [8]. The grain morphology of IN718 specimens produced at 1000, 1068, 1150, and 1200 °C sintering temperatures under 50 and 60 MPa pressures is shown Fig. 7. The grain size measurements were made on a representative area of each specimen in order to assess the influence of temperature on the growth of grains. Therefore, in the hot-pressed IN718 specimens sintered at 1000 °C, a small number of grains grew little and were not measured because they are not representative of the fracture mode observed.

The grain morphology's analysis allowed us to infer that the high sintering temperatures lead to an increase in the grain size and, consequently, a boost on the crystallinity. The defined temperature of 1000 °C was not sufficient to potentiate nucleation and growth of the grains. T1000P50 and T1000P60 (see Fig. 7) presented large particles scattered with small particles and prior particle boundaries with no observed atomic diffusion (normally driven by elevated sintering temperatures). A weakly particles bonding was observed at both T1000P50 and T1000P60 specimens with punctual contact points (usually called necks) due to a low free energy surface that prevents the powder particles' connection by atomic diffusion and, consequently, the creation of voids. When increasing the temperature to 1068 °C, it is possible to observe the grains already nucleated in which the total recrystallization of some grown grains. The recrystallization was achieved when the surface contact stress was progressively decreased, and the contacted powders stick to each other, and the aforesaid voids disappeared. IN718 specimens manufactured at 1150 °C and 1200 °C showed a superior homogenized grain size with nucleation and growth with grain size of 11.76 and 17.22 µm (for 60 MPa), respectively.

3.5 Hardness

The influence of temperature on hardness properties was also studied in IN718 specimens sintered at 1000, 1068, 1150, and 1200 °C.

The lower hardness values, 200 and 213 HV, were achieved when considering the lowest sintering temperature (1000 °C) for 50 and 60 MPa, respectively. Even though the XRD pattern has revealed the existence of hardening phases such as Nb carbides (NbC and Nb_4C), the low hardness results are attributed to the weakly powder bonding (see fracture surface in Fig. 5)

The hardness values decreased when increasing the temperature from 1068 to 1150 °C since the increase on grain size led to a decrease on low hardness values. It occurred because the large grains have a lower amount of grain boundaries and so low quantity of dislocations. The increase on temperature values is important not only for the metallurgical bonding (by enhancing the atomic diffusion) but also for the element's precipitation and solubilization. XRD patterns showed that chromium carbides ($Cr_{23}C_6$) were precipitated at 1068 °C and dissolved at 1150 °C (for 60 MPa). As it is known that carbides improve the hardness values, the reduction of the quantity of chromium carbides ($Cr_{23}C_6$) with the increase in temperature may lead to a decrease in hardness results (from 275 to 255 HV) under 60 MPa of pressure [26].

The hardness results revealed a significant improvement when increasing the sintering temperature to 1200 °C (327 HV). These results are coherent with the densification obtained (close to 100%) and the fracture surface (see Fig. 8).

Table 4 presents hardness results of IN718 specimens produced by other technologies such as SLM and

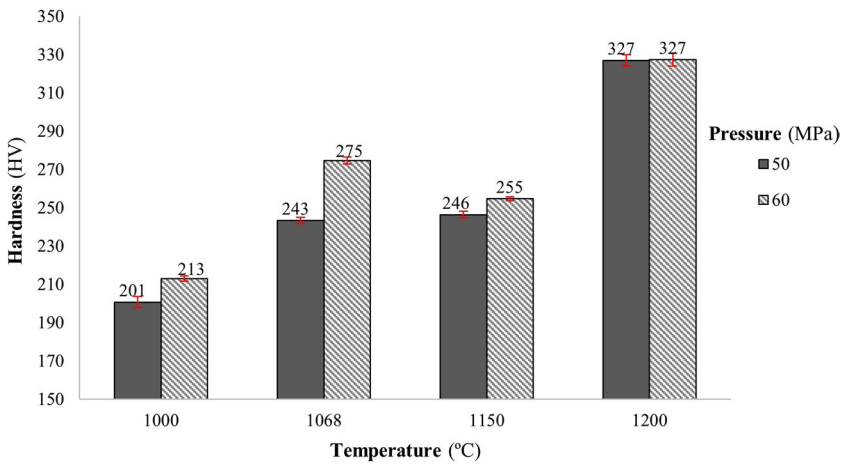

Fig. 8 Hardness results of IN718 specimens

Table 4 Hardness results, in Vickers (HV), of IN718 specimens manufactured by several engineering methods (Bot, bottom; Top; Ver, vertical)

Manufacturing process	Hardness (HV)	Ref.
This study	**327** (1000 g load)	-
As-SLMed	Bot (**211**), Top (**205**), Ver (**237**) (50-g load)	[28]
As-SLMed + homogenization	Bot (**289**), Top (**260**), Ver (**283**) (50-g load)	
As-SLMed + HIP	Bot (**181**), Top (**176**), Ver (**181**) (50-g load)	
Laser deposition	**275–350** (300 g)	[29]
Field-assisted hot pressing (FAHOT pressing)	**256** (1000 g)	[30]
Microwave sintering	**191** (1000 g)	
Metal injection molding	**211** (1000 g)	

The entries in boldface are the hardness values

laser deposition to compare with those obtained in this study. Generally, the hardness results were lower than those reported in this study. Seede et al. [28] studied the microhardness of as-built SLMed specimens and as-built SLMed with posterior homogenization (1100 °C, 1 h) and hot isostatic pressing (1160 °C, 100 MPa, 4 h). The as-built SLMed specimen and the homogenized specimens revealed hardness values of 237 and 283 HV, respectively. The as-built specimen hardness was 19. 3% lower than the homogenized due to the nucleated small grains and greater dissemination of secondary precipitation. In this study, the T1000P50 and T1000P60 specimens (with a lower quantity of smaller grains nucleated) revealed lower hardness results (201 and 213 HV at 50 and 60 MPa, respectively) than the abovementioned results. This occurred due to the low densification of these specimens with poor diffusion and the presence of some voids.

The IN718 specimens subjected to homogenization showed higher hardness results (292 HV) and so closer to values to those achieved in this work. The large dispersion of $\gamma''(Ni_3Nb)$ precipitates were responsible for the high hardness results obtained, showing the existence of 100% of γ(CrNi) on XRD pattern. In coherence with that, the hot-pressed specimens also showed the γ phase when sintered at comparable temperature (1068 °C) as well the hardenable chromium carbides (NbC and Nb_4C_3) derived from the huge macrosegregation of Nb during cooling and solidification. On the opposite, the HIPed specimens revealed low hardness values than as-built and homogenized specimens. At high temperature and pressure conditions, there was verified a high dissolution of γ'' phase and so a significant decrease in the hardness results. Zhang et al. [29] assessed the microhardness results of IN718 specimens produced through a fibre laser deposited filler wire and also showed that the main strengthening phase γ'' was dissolved during the laser cladding that led a lower hardness value than the IN718 specimens which were heat treated and aged. Dugauguez et al. [30] assessed hardness results of IN718 specimens between three different manufacturing processes. In fact, as the indentation load/size effect (ISE) has a strong influence on hardness results, the authors did not establish a relation with the microhardness results [31]. The IN718 specimens manufacturing by FAHOT pressing revealed hardness results of 256 HV, so lower than the remaining processes. The IN718 specimens produced by microwave sintering technique revealed lower hardness results (191 HV) than the remaining results due to the existence of surface cracks [30]. The violent debinding and the existence of hot spots in the interior of the specimens were responsible for these cracks.

In this study, the occurrence of defects (e.g., voids) led to low hardness results such as specimens produced at 1000 °C. The hardness results increased with the temperature due to the precipitation of some elements combined with the enhancement of atomic diffusion and so powder consolidation.

4 Conclusions

The present study showed that the increase of temperature has a great influence on the densification results of IN718 parts produced by uniaxial vacuum hot pressing.

- The hot-pressed IN718 specimens that consider the lowest sintering temperature showed lack of plastic deformation and atomic diffusion.
- The densification levels achieved values close to 100%.
- IN718 specimens revealed an acceptable metallurgical bonding since the fracture mode presented was a fully ductile dimple fracture.
- Well-sintered specimens at high temperatures presented grown grains with a grain size homogeneity.
- At high temperature evaluated of 1200 °C, the optimum hardness results were achieved (327 HV).

In future studies, the hot-pressing conditions should embrace a large range of sintering conditions in order to deeply evaluate its impact on densification. Furthermore, the mechanical tests should include the evaluation of shear and tensile strength.

Author contribution Ana Marques: conceptualization; formal analysis; methodology; investigation; and writing—original draft. Ângela Cunha: conceptualization; methodology; writing—review and editing; and supervision. Flávio Bartolomeu: investigation and writing—review and editing. Filipe Silva: project administration; funding acquisition; resources; and supervision. Óscar Carvalho: conceptualization; methodology; and writing—review and editing.

Funding Open access funding provided by FCT|FCCN (b-on). This work was supported by FCT (Fundação para a Ciência e Tecnologia) through the grant national funds, under the national support to R&D unit grant, through the reference projects UIDB/04436/2020 and UIDP/04436/2020 and SFRH/BD/148031/2019. This work was also cofinanced by FEDER, through the Competitiveness and Internationalization Operational Program (POCI), in the project Add. Additive, with the reference POCI-01-0247-FEDER-024533.

Data availability All data used in this work have been properly cited within the article.

Code availability Not applicable.

Declarations

Ethics Not applicable.

Consent to participate The authors declare that all authors have read and approved to submit this manuscript to IJAMT.

Consent for publication The authors declare that all authors agree to sign the transfer of copyright for the publisher to publish this article upon on acceptance.

Conflict of interest The authors declare no competing interests.

References

1. Boyer RR, Cotton JD, Mohaghegh M, Schafrik RE (2015) Materials considerations for aerospace applications. Mater Eng Propelling Innov 40(1055-1066):1055–1066. https://doi.org/10.1557/mrs.2015.278
2. Fecht H, Fecht H (2000) Processing of nickel-based superalloys for turbine engine disc applications. Adv Eng Mater 12:777–787. https://doi.org/10.1002/1527-2648
3. Sutton GP, Ross DM, Oscar. (2001) Biblarz, Rocket propulsion elements, 7th ed. John Wiley & Sons
4. M. Pizzarelli, Regenerative cooling of liquid rocket engine thrust chambers, (n.d.). https://www.researchgate.net/publication/321314974_Regenerative_cooling_of_liquid_rocket_engine_thrust_chambers (Accessed Feb. 12, 2022)
5. Dowson G, Whittaker D (2008) Introduction to Powder Metallurgy The Process and Its Products. Eur Powder Metall Assoc 36:4–20. https://doi.org/10.1017/CBO9781107415324.004
6. Mouritz AP (2012) Introduction to Aerospace Materials. In: Introduction to Aerospace Materials, 1st ed. Publishing, Woodhead, pp 1–14. https://doi.org/10.1533/9780857095152.1
7. Hot Isostatic Pressing (HIP), European Powder Mettalurgy Association, (n.d.). https://www.epma.com/hot-isostatic-pressing (Accessed Feb. 15, 2022)
8. Chang SH, Lee SC, Tang TP, Ho HH (2006) Evaluation of HIP pressure on Inconel 718 superalloy. Int J Cast Met Res 19:181–187. https://doi.org/10.1179/136404606225023408
9. Chang SH, Lee SC, Tang TP, Ho HH (2006) Effects of temperature of HIP process on characteristics of Inconel 718 superalloy. Int J Cast Met Res 19:175–180. https://doi.org/10.1179/136404606225023399
10. Bartolomeu F, Buciumeanu M, Pinto E, Alves N, Silva FS, Carvalho O, Miranda G (2017) Wear behavior of Ti6Al4V biomedical alloys processed by selective laser melting, hot pressing and conventional casting. Trans Nonferrous Metals Soc China 27:829–838. https://doi.org/10.1016/S1003-6326(17)60060-8
11. Madeira S, Pinto AMP, Rodrigues LC, Carvalho O, Miranda G, Reis RL, Caramês J, Silva FS (2017) Effect of sintering pressure on microstructure and mechanical properties of hot-pressed Ti6Al4V-ZrO2 materials. Mater Des 120:394–403. https://doi.org/10.1016/j.matdes.2017.02.038
12. Andrew Ruys SM, Gingu O, Sima G (2015) Powder Processing of Bulk Components in Manufacturing. In: Handbook of Manufacturing Engineering and Technology. Springer, London, pp 487–566. https://doi.org/10.1007/978-1-4471-4670-4_48
13. Brian James W (2015) Powder Metallurgy Methods and Applications. In: Powder Metallurgy, 1st ed. ASM International, pp 9–19. https://doi.org/10.31399/asm.hb.v07.a0006022
14. Chang L, Sun W, Cui Y, Yang R (2014) Influences of hot-isostatic-pressing temperature on microstructure, tensile properties and tensile fracture mode of Inconel 718 powder compact. Mater Sci Eng A 599:186–195. https://doi.org/10.1016/j.msea.2014.01.095
15. German RM (2014) Sintering With External Pressure. In: Sintering: From Empirical Observations to Scientific Principles, 1st ed., pp 305–354. https://doi.org/10.1016/b978-0-12-401682-8.00010-0
16. Ha HY, Lee TH, Bae JH, Chun DW (2018) Molybdenum effects on pitting corrosion resistance of FeCrMnMoNC austenitic stainless steels. Metals 8:1–13. https://doi.org/10.3390/met8080653
17. Suwardie JH, Artiaga R, Mier JL (2002) Thermal characterization of a Ni-based superalloy. Thermochim Acta 392–393:295–298. https://doi.org/10.1016/S0040-6031(02)00112-0
18. Technical Data Sheet CT Powder Range 718, Carpenter Additive. (2019). https://cdn2.hubspot.net/hubfs/6205315/carpenter_additive/image/Resources/Datasheets/CT-PowderRange-718-E.pdf. Accessed 4 Apr 2022
19. High-Performance Nickel Alloys - the Alloy Specialists, Special Metals, (n.d.). www.specialmetals.com. Accessed 16 Mar 2022
20. Caliari FR, Candioto KCG, Pereira Reis DA, Couto AA, de Moura Neto C, Nunes CÂ (2015) Effect of aging treatment 0n inconel 718 superalloy: application in elevated temperatures. Mater Sci Forum 805:199–203. https://doi.org/10.4028/www.scientific.net/MSF.805.199
21. Elrakayby H, Kim HK, Hong SS, Kim KT (2015) An investigation of densification behavior of nickel alloy powder during hot isostatic pressing. Adv Powder Technol 26:1314–1318. https://doi.org/10.1016/j.apt.2015.07.005

22. Marsh C (2018) The Mechanical Properties and Deformation Behavior of Heat Treated Versus As-Received Inconel X-750. University of South Carolina
23. Sun W, Tan AWY, Wu K, Yin S, Yang X, Marinescu I, Liu E (2020) Post-process treatments on supersonic cold sprayed coatings: A review. Coatings 10:123. https://doi.org/10.3390/coatings10020123
24. Chaturvedi MC, Han Y (1983) Strengthening mechanisms in Inconel 718 superalloy, Metal. Science 17:145–149. https://doi.org/10.1179/030634583790421032
25. Niang A, Viguier B, Lacaze J (2010) Some features of anisothermal solid-state transformations in alloy 718. Mater Charact 61:525–534. https://doi.org/10.1016/j.matchar.2010.02.011
26. Peasura P, Poopat B (2015) Investigation into the influence of post-weld heat treatment on the microstructure and hardness of inconel X-750. Adv Mech Eng 7:1–11. https://doi.org/10.1177/1687814015578396
27. Sugahara T, Couto AA, Barboza MJR, Neto FP, Takahashi RJ, Reis DAP (2022) Creep and mechanical behavior study of Inconel 718 Superalloy. Mater Res 25:1–9. https://doi.org/10.1590/1980-5373-MR-2021-0280
28. Seede R, Mostafa A, Brailovski V, Jahazi M, Medraj M (2018) Microstructural and microhardness evolution from homogenization and hot isostatic pressing on selective laser melted inconel 718: structure, texture, and phases. J Manuf Mater Process 2:30. https://doi.org/10.3390/jmmp2020030
29. Kistler NA, Nassar AR, Reutzel EW, Corbin DJ, Beese AM (2017) Effect of directed energy deposition processing parameters on laser deposited Inconel ® 718: microstructure, fusion zone morphology, and hardness. J Laser Appl 29:022005. https://doi.org/10.2351/1.4979702
30. Dugauguez O, Torralba JM, Barriere T, Gelin JC (2016) Unconventional methods of sintering inconel 718 MIM Samples. Key Eng Mater 716:830–839. https://doi.org/10.4028/www.scientific.net/KEM.716.830
31. Milman YV, Golubenko AA, Dub SN (2011) Indentation size effect in nanohardness. Acta Mater 59:7480–7487. https://doi.org/10.1016/j.actamat.2011.08.027